group. The simultaneous presence of basic oxide atoms and an unionized acidic hydroxyl is unusual but is generally consistent with V–O–As bonds being weaker than V–O–P bonds as suggested by the higher solubilities observed for vanadium arsenates compared with those of vanadium phosphates. The effect of intralayer hydrogen bonding and steric factors associated with packing the phenyl groups in the interlayer space must also be important in determining the final composition and structure. Further comparative studies of vanadyl organophosphonate and arsonate structures are in progress.

Acknowledgment. We thank D. P. Goshorn for the magnetic susceptibility measurements.

Registry No. $V_2O_4(C_6H_5AsO_3H)\cdot H_2O$, 130063-84-2; $C_6H_5AsO_3H_2$, 98-05-5; V_2O_3, 1314-34-7.

Supplementary Material Available: Tables of anisotropic thermal parameters, bond angles, and hydrogen atom coordinates (2 pages); observed and calculated structure factors (9 pages). Ordering information is given on any current masthead page.

Magnetic Exchange Interactions in One-Dimensional Copper(II) Compounds

Pere Alemany and Santiago Alvarez*

Departament de Química Inorgànica, Universitat de Barcelona, Diagonal 647, 08028 Barcelona, Spain

Received June 8, 1990

A theoretical study is presented of the weak magnetic exchange interaction in one-dimensional halo-bridged pentacoordinate Cu(II) complexes with $CuY_3(\mu\text{-}X)$ and $CuY_2(\mu\text{-}X)_2$ cores for the repeat unit (X = Cl, Br), in which the arrangement of the ligands around the copper atoms can vary from trigonal bipyramidal to square pyramidal to pseudooctahedral. Electronic band structure calculations of the extended Hückel type were performed on the model chain compounds $[CuCl_3(\mu\text{-}Cl)]_n^{2-}$, $[CuBr_3(\mu\text{-}Br)]_n^{2-}$, and $[CuCl_2(\mu\text{-}Cl)_2]_n^{2-}$, and the dependence of the bandwidth (W) of the highest occupied band on the structural parameters is studied. The largest values of W occur for the trigonal-bipyramidal geometry and a large Cu–bridge–Cu angle ($\varphi \sim 180°$), whereas W is practically constant and small for a square pyramid and small bridging angles, in good qualitative agreement with the experimental coupling constants.

The study of magnetic exchange interactions between transition-metal ions in dimers and in chains has been an area of constant interest during the past two decades.[1] Copper(II) complexes, with one unpaired electron per copper atom, provide the simplest case study, yet the geometries available to such complexes make them a rich field for both experimental and theoretical research.

A particular case of Cu(II) chain complexes showing weak magnetic coupling is that of halo-bridged pentacoordinate complexes with $CuY_3(\mu\text{-}X)$ or $CuY_2(\mu\text{-}X)_2$ cores for the repeat unit (X = Cl, Br). In the singly bridged chains, long Cu–X bonds occupy either the apical position of a square pyramid or one of the equatorial sites of a trigonal bipyramid,[2-6] with an idealized local symmetry C_{2v} around the Cu atom. The geometrical parameters that define such structures are shown in **1**: an angle δ of $\sim 180°$ corresponds to a square pyramid with the bridging ligand coordinated to neighboring copper atoms in axial (longer Cu–Cl bond distance) and equatorial positions, respectively. A value of $\delta \sim 120°$, on the other hand, corresponds to a trigonal bipyramid with the bridging ligand occupying

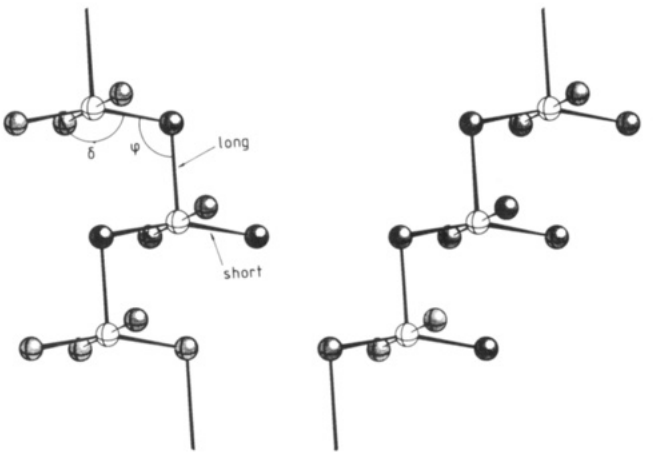

1 **2**

equatorial positions of two copper atoms. The bridging angle φ is also found to vary in the range 114–145°. Notice that in **1** there are two Cu atoms per repeat unit. For linear chains **2**, with one Cu per unit cell[7-9] both angles are related through the equation $\delta = 360° - 2\varphi$.

A particular situation occurs when $\varphi \approx 90°$ and $\delta \approx 180°$ in structures **1** and **2**. Then, the ligand under the equa-

(1) Willett, R. D., Gatteschi, D., Kahn, O., Eds. *Magneto-Structural Correlations in Exchange Coupled Systems*; D. Reidel: Dordrecht, 1985.
(2) Bream, R. A.; Estes, E. D.; Hodgson, D. J. *Inorg. Chem.* **1975**, *14*, 1672.
(3) Lundberg, B. K. S. *Acta Chem. Scand.* **1972**, *26*, 3977.
(4) Willett, R. D.; Chang, K. *Inorg. Chim. Acta* **1970**, *4*, 447.
(5) Watkins, N. T.; Jeter, D. Y.; Hatfield, W. E.; Horner, S. M. *Trans. Faraday Soc.* **1971**, *67*, 2431.
(6) Bandoli, G.; Biagini, M. C.; Clemente, D. A.; Rizzardi, G. *Inorg. Chim. Acta* **1976**, *20*, 71.
(7) Sheldrick, W. S.; Bell, P. *Z. Naturforsch.* **1987**, *42b*, 195.
(8) Rojo, T.; Mesa, J. L.; Arriortua, M. I.; Savariault, J. M.; Galy, J.; Villeneuve, G.; Beltrán, D. *Inorg. Chem.* **1988**, *27*, 3904.
(9) Folgado, J. V.; Coronado, E.; Beltrán, D.; Burriel, R.; Fuertes, A.; Miravitlles, C. *J. Chem. Soc., Dalton Trans.* **1988**, 3041.

0897-4756/90/2802-0723$02.50/0

Table I. Geometrical and Magnetic Parameters for Cu(II) Chain Compounds of Types 1 and 2[a]

	compd[b]	structure	core of repeat unit	δ, deg	φ, deg	J_{exp} cm^{-1}	W, meV	J_{calc}, cm^{-1}	ref
a	*trans*-[Cu(dmso)Cl_2]	1	*trans*-$O_2Cl(\mu$-Cl)	146	145	−6.1	133	−3.99	4, 24
b	*trans*-[Cu(Im)Cl_2]	1	*trans*-$N_2Cl(\mu$-Cl)	167	117	−2.1	7	−0.01	3, 24
c	*trans*-[Cu(caffeine)Cl_2]	1	*trans*-NOCl(μ-Cl)	179	128	0.48	0	0.00	6, 24
d	*cis*-[Cu(maep)Cl_2]	1	*cis*-$N_2Cl(\mu$-Cl)	166	114	1.58	2	0.00	2, 24
e	[Cu(oaoH$_2$)Cl_2]	2	*cis*-$N_2Cl(\mu$-Cl)	166	96	−1.0	34	−0.26	8
f	[Cu(paphy)Cl](PF_6)·H_2O	1	$N_3(\mu$-Cl)	168	102	0.5	21	−0.10	25
g	[Cu(pcpci)Cl]	2	$N_3(\mu$-Cl)			−0.4			9
h	[Cu(allH$_3$)Cl_3]	1	$NCl_2(\mu$-Cl)	154	112		12	−0.03	7
i	[Cu(H_2O)(mallH)Cl_2]	2	*trans*-NOCl(μ-Cl)	169	97		30	−0.21	7
j	[Cu(dmso)$_2$$Br_2$]	1	*trans*-$O_2Br(\mu$-Br)	146	145	−7.9	379	−33.3	8
k	[Cu(pcpci)Br]	2	$N_3(\mu$-Br)	165	94	−0.8	40	−0.38	9

[a] W and J_{calc} are the calculated bandwidths and coupling constants (eq 2) for the model chain compound $[\mu$-$CuCl_3]_n$ with structure 1. [b] dmso = dimethyl sulfoxide; ImH = imidazole; maep = 2-(2-(methylamino)ethyl)pyridine; paphy = pyridine-2-carboxaldehyde; oaoH$_2$ = oxamide oxime; pcpci = *N*-(2′-pyridylcarbonyl)pyridinyl-2-carboximidate; allH$_2$ = allopurinol; mallH = 9-methylallopurinol.

torial plane of a square pyramid becomes close enough to the copper atom as to complete a pseudooctahedral coordination. Structure 1 thus becomes a ladder **3**, and

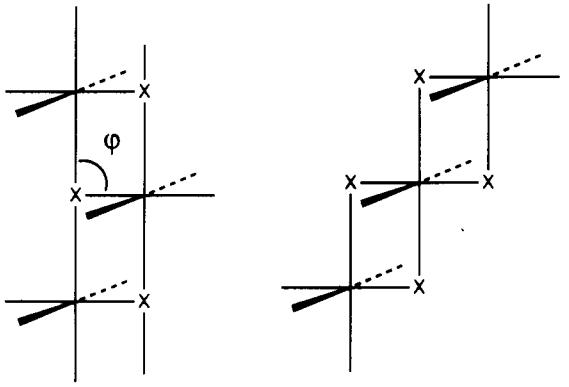

3 **4**

structure 2 becomes a regular edge-sharing chain of elongated octahedra **4**. There is still a related structure, a zigzag chain of octahedra **5**. The Cu(μ-X)$_2$Cu framework is usually distorted from the ideal structures **3**–**5** (i.e., $\varphi \neq 90°$). Hence, **3** becomes **6**, and similarly for **4** and **5**.

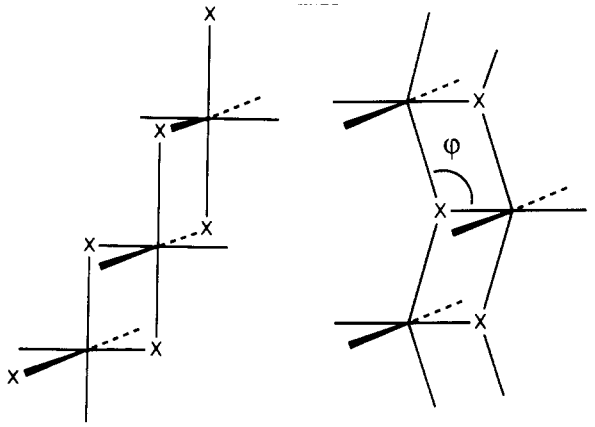

5 **6**

The coupling constants of such chain compounds and their geometrical parameters δ and φ are shown in Tables I and II. Other compounds of this family have been reported, but their structures were not determined.[10] The aim of the present work is to theoretically study how both geometrical parameters affect the magnitude of the exchange interaction. Thus electronic band structure calculations[11] of the extended Hückel type[12] were performed on model chain compounds $[CuY_3(\mu$-$X)]_n^{2-}$ and $[CuY_2(\mu$-$X_2)]_n^{2-}$ (X, Y = Cl, Br; see Appendix for computational details).

Dependence of Bandwidths on the Geometry. Systems with partially filled bands can behave in different ways, including Peierls distortions from ideal symmetry, metallic, ferromagnetic, or antiferromagnetic states.[13] Although it is not easy to evaluate the relative energies of such states, the qualitative trends within a family of one-dimensional compounds can be rationalized with a one-electron model[14-17] in much the same way that it has been applied to dinuclear complexes.[18]

Roughly speaking, wide partially filled bands should be associated with either metallic behavior or Peierls distortions, whereas narrow partially filled bands are typical of ferromagnetic or antiferromagnetic compounds.[13] A ferromagnetic state is favored for small bandwidths, while the strength of antiferromagnetic interactions increases with the square of the bandwidth. Girerd, Charlot, and Kahn[19,20] expressed the magnetic coupling constant, J, as a sum of both ferromagnetic and antiferromagnetic contributions, J_F and J_{AF}, respectively. The antiferromagnetic contribution can be approximated as

$$J_{AF} \approx \frac{1}{n^2} \sum_{\mu=1}^{n} \frac{W_\mu^2}{3\epsilon_\mu} \qquad (1)$$

where n is the number of unpaired electrons per atom, ϵ_μ is the mean energy of each partially filled band, and W_μ is its bandwidth. In the present case, there is one unpaired electron per copper atom (n = 1), and eq 1 becomes

$$J_{AF} \approx W^2/3\epsilon \qquad (2)$$

The ferromagnetic contribution, J_F, is usually considered to be approximately constant for a series of analogous

(10) van Ooijen, J. A. C.; Reedijk, J. *J. Chem. Soc., Dalton Trans.* **1978**, 1170.

(11) (a) Whangbo, M.-H.; Hoffmann, R. *J. Am. Chem. Soc.* **1978**, *100*, 6093. (b) Whangbo, M.-H.; Hoffmann, R.; Woodward, R. B. *Proc. Roy. Soc. London, Ser. A* **1979**, *366*, 23.

(12) (a) Hoffmann, R. *J. Chem. Phys.* **1963**, *39*, 1397. (b) Hoffmann, R.; Lipscomb, W. N. *J. Chem. Phys.* **1962**, *36*, 2179, 2872, 3489.

(13) Whangbo, M.-H. *Acc. Chem. Res.* **1983**, *16*, 95. Whangbo, M.-H. *J. Chem. Phys.* **1980**, *73*, 3854. Whangbo, M.-H. *J. Chem. Phys.* **1981**, *75*, 4983.

(14) Whangbo, M.-H.; Foshee, M. J.; Hoffmann, R. *Inorg. Chem.* **1980**, *19*, 1723.

(15) Kahn, O. *Angew. Chem., Int. Ed. Engl.* **1985**, *24*, 834.

(16) Charlot, M.-F.; Girerd, J.-J.; Kahn, O. *Phys. Status Solidi* **1978**, *86*, 497.

(17) Sherwood, P.; Hoffmann, R. *Inorg. Chem.* **1989**, *28*, 509.

(18) Hay, P. J.; Thibeault, J. C.; Hoffmann, R. *J. Am. Chem. Soc.* **1975**, *97*, 4884.

(19) Charlot, M.-F.; Girerd, J.-J.; Kahn, O. *Phys. Status Solidi* **1978**, *86b*, 497.

(20) Girerd, J.-J.; Charlot, M.-F.; Kahn, O. *Mol. Phys.* **1977**, *34*, 1063.

Table II. Geometrical and Magnetic Parameters for Cu(II) Chain Compounds of Types 3-5[a]

	compd	structure	core of repeat unit	r, Å	φ, deg	J_{exp}, cm^{-1}	ref
m	$[Cu(py)Cl_2]$	4	*trans*-$N_2Cl_2(\mu\text{-}Cl)_2$	3.03	91.5	-9.2	28-30
n	$[Cu(4\text{-}Etpy)_2Cl_2]$	4	*trans*-$N_2Cl_2(\mu\text{-}Cl)_2$	3.22	91.8	-6.7	29, 31
p	$[Cu(4Vpy)_2Cl_2]$	4	*trans*-$N_2Cl_2(\mu\text{-}Cl)_2$	3.10	90.0	-9.1	29, 32
q	$[Cu(tz)_2Cl_2]$	4	*trans*-$N_2Cl_2(\mu\text{-}Cl)_2$	3.00	91.9	-3.8	33
r	$[Cu(H_2O)_2Cl_2]$	4	*trans*-$O_2Cl_2(\mu\text{-}Cl)_2$	2.94	88.8	-4.9	34-36
s	$[Cu(N_2H_5)Cl_3]$	3	*trans*-$NCl_3(\mu\text{-}Cl)_2$	2.85	92.8	-3.2	37
t	$[Cu(dpg)Cl_2]$	5	*cis*-$N_2Cl_2(\mu\text{-}Cl)_2$	2.90	89.3	0.7	38
u	$[Cu(paphy)Br](PF_6)\cdot H_2O$	3	*trans*-$N_3Br(\mu\text{-}Br)_2$	3.36	81.7	~0.0	8
v	$[Cu(py)Br_2]$	4	*trans*-$N_2Br_2(\mu\text{-}Br)_2$	3.24	89.6	-18.9	28-30
w	$[Cu(MeIm)_2Br_2]$		*trans*-$N_2Br_2(\mu\text{-}Br)_2$			-14.3	10
x	$[Cu(tz)_2Br_2]$					-10.4	33
y	$[Cu(ampy)Br_2]$	3	*cis*-$N_2Br_2(\mu\text{-}Br)_2$	3.26	80.8		39
z	$[Cu(Metmen)Br_2]$	3	*cis*-$N_2Br_2(\mu\text{-}Br)_2$	3.11	87.6		39

[a] py = pyridine; 4-Etpy = 4-ethylpridine; 4-Vpy = 4-vinylpyridine; tz = thaizole; dpg = diphenylgyloximate; paphy = pyridine-2-carboxaldehyde; MeIm = *N*-methylimidazole; ampy = 2-(2-aminomethyl)pyridine; Metmen = 2-methyl-1,2-diaminopropane.

compounds. Recent ab initio calculations on dinuclear Cu(II) complexes show that the variations of the calculated J with geometry nicely follow the changes in the antiferromagnetic contribution.[21-23] Hence a rough estimate of the geometry dependence of J can be obtained by calculating ϵ_μ and W at the extended Hückel level. Therefore, in the family of compounds with structural types 1 and 2, any factor contributing to a wide highest occupied band (HOB) will favor the antiferromagnetic coupling and vice versa, with very narrow bands ($J_{AF} \approx 0$) eventually giving rise to ferromagnetism.

Singly Bridged Chains. If one considers the case of a square-pyramidal coordination environment around a Cu(II) ion, the unpaired electron is expected to be located in its $d_{x^2-y^2}$ orbital. In the one-dimensional compounds of type 1 with $\delta \sim 180°$, a half-filled band formed from the combinations of such orbitals should be the HOB. Similarly, the highest occupied MO for the trigonal bipyramidal structure is mainly d_{z^2}, with antibonding contributions from the ligands' σ-donor orbitals. Therefore, in the chains 1 with $\delta \sim 120°$, the HOB bearing unpaired electrons must be the z^2 band. The gradual change of the $x^2 - y^2$ orbital to z^2 when δ changes from 180 to 120° has been previously described.[27]

The dispersion relationships for the d-block bands of $[CuBr_3(\mu\text{-}Br)]^{2-}_n$ with structure 1 in a trigonal-bipyramidal geometry (δ = 120°) and a bridging angle φ = 150°. The block representation of the HOB indicates that it is half-filled but has no implications on the occupation or spin of each level in that band.

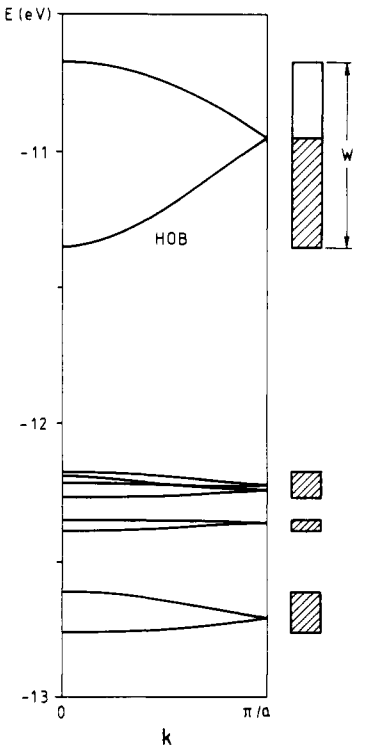

Figure 1. Band structure diagram for the d block of $[CuBr_3(\mu\text{-}Br)]^{2-}_n$ with structure 1 in a trigonal-bipyramidal geometry (δ = 120°) and a bridging angle φ = 150°. The block representation of the HOB indicates that it is half-filled but has no implications on the occupation or spin of each level in that band.

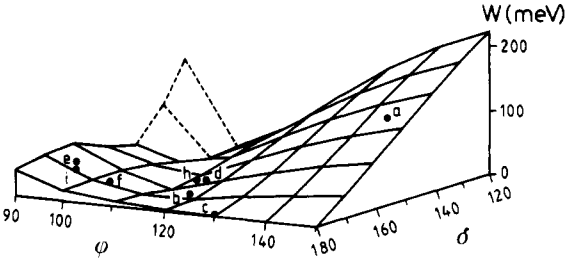

Figure 2. Width of the highest occupied band (HOB) as a function of the structural parameters defined in 1. The points indicate the angles corresponding to experimental structural data collected in Table I.

$[CuBr_3(\mu\text{-}Br)]_n^{2-}$ in the trigonal bipyramidal structure 1 (δ = 120°, φ = 150°) are shown in Figure 1. The HOB is built up from the d_{z^2} orbitals of the Cu atoms with antibonding contributions from the ligands, as discussed above, and is well separated from the rest of the d bands. The

(21) Astheimer, H.; Haase, W. *J. Chem. Phys.* **1986**, *85*, 1427.
(22) Handa, M.; Koga, N.; Kida, S. *Bull. Chem. Soc. Jpn.* **1988**, *61*, 3853.
(23) For a discussion on the relationship between qualitative (EH) and ab initio results, see: Alvarez, S.; Julve, M.; Verdaguer, M. *Inorg. Chem.*, in press, and references therein.
(24) Estes, W. E.; Hatfield, W. E.; van Ooijen, J. A. C.; Reedijk, J. *J. Chem. Soc., Dalton Trans.* **1980**, 2121.
(25) Endres, H.; Nöthe, D.; Rossato, E.; Hatfield, W. E. *Inorg. Chem.* **1984**, *23*, 3467.
(26) Willet, R. D.; Jardine, F. H.; Roberts, S. A. *Inorg. Chim. Acta* **1977**, *25*, 97.
(27) Albright, T. A.; Burdett, J. K.; Whangbo, M.-H. *Orbital Interactions in Chemistry*; Wiley: New York, 1985.
(28) Jeter, D. Y.; Hatfield, W. E. *J. Inorg. Nucl. Chem.* **1972**, *34*, 3055.
(29) Marosin, B. *Acta Crystallogr., Sect. B* **1975**, *B31*, 632.
(30) Crawford, V. H.; Hatfield, W. E. *Inorg. Chem.* **1977**, *16*, 1336.
(31) Laing, M.; Garr, G. *J. Chem. Soc. A* **1971**, 1141.
(32) Laing, M.; Harsfield, E. *J. Chem. Soc., Chem. Commun.* **1968**, 735.
(33) Estes, W. E.; Gavel, D. P.; Hatfield, W. E.; Hodgson, D. J. *Inorg. Chem.* **1978**, *17*, 1415.
(34) Losee, D. B.; McElearney, J. N.; Siegel, A.; Carlin, R. L.; Khan, A. A.; Roux, J. P.; James, W. J. *Phys. Rev., Sect. B* **1972**, *B6*, 4342.
(35) Harker, D. *Z. Kristallogr.* **1936**, *93*, 136.
(36) Engberg, A. *Acta Chem. Scand.* **1970**, *24*, 3510.
(37) Brown, D. B.; Donner, J. A.; Hall, J. W.; Wilson, S. R.; Wilson, R. B.; Hodgson, D. J.; Hatfield, W. E. *Inorg. Chem.* **1978**, *18*, 2635.
(38) Mêgnamisi-Bélombé, M.; Singh, P.; Bolster, D. E.; Hatfield, W. E. *Inorg. Chem.* **1984**, *23*, 2578.
(39) Helis, H. M.; Goodman, W. H.; Wilson, R. B.; Morgan, J. A.; Hodgson, D. J. *Inorg. Chem.* **1977**, *16*, 2412.

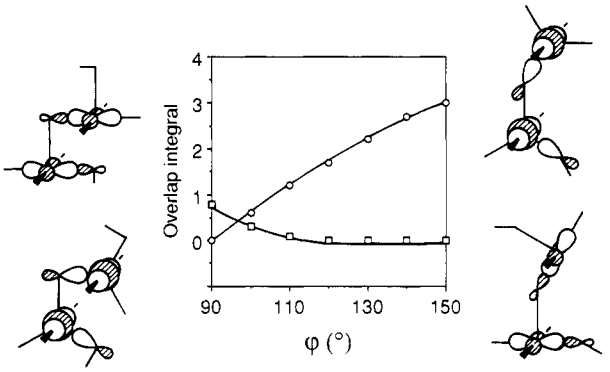

Figure 3. Overlap integrals ($\times 10^3$) between the HOMOs of two $[CuCl_4]^{2-}$ units in a dimer with a square-pyramidal (circles) or a trigonal-bipyramidal structure (squares), as a function of the bridging angle φ.

lowest level of the HOB has bonding character for the long Cu–X bond (see Figure 3, upper right corner), whereas the highest level of the same band is Cu–X antibonding. It is thus obvious that geometry changes can modify the separation between both levels (i.e., the bandwidth W). In fact, calculations using different geometries or substituting Cl for Br give qualitatively the same band diagram but different bandwidths for the HOB.

Although the long Cu–X bond distance should also affect the bandwidth, this distance is practically constant for all chloro-bridged chains (compounds a–i in Table I), and we need to focus only on the effect of the bond angles φ and δ. The bandwidths calculated for the model chain, $[CuCl_3(\mu\text{-}Cl)]_n^{2-}$ with structure **1**, as a function of δ and φ, are plotted in Figure 2. Parallel calculations were carried out for the same model with structure **2**, and the results were practically identical, indicating that the bandwidth of the HOB is largely determined by nearest-neighbor interactions. In Figure 2 the largest values of W occur for $\delta \sim 120°$ and $\varphi \sim 150°$, whereas it is practically constant and small when $\delta \sim 180°$ (i.e., for a square pyramid) and when the bridging angle is small ($\varphi \sim 100°$). The relatively large values of W found in the region close to $\delta = 120°$, $\varphi = 90°$ (dashed lines in Figure 2) are just an artifact of the model due to the strong four-electron repulsions resulting from ligands in neighboring unit cells at a too short distance ($\sim$2.4 Å). The trends reflected in Figure 2 are in good qualitative agreement with the experimental coupling constants shown in Table I. In Table I it can be seen that the compound with the strongest antiferromagnetic coupling (compound a) has not only the geometry closest to a trigonal bipyramid but also the largest bridging angle φ. For the sake of comparison, the (φ, δ) pairs corresponding to the experimental structures are represented in Figure 2 by circles. A similar plot is obtained for the bromo-bridged model chain, $[CuBr_3(\mu\text{-}Br)]_n^{2-}$, only with a larger slope in the δ direction. The two bromo-bridged compounds (j and k in Table I) also agree with the qualitative predictions: j is located on the hill of Figure 2, where larger antiferromagnetic coupling constants are expected, whereas k is on the valley, with practically no magnetic coupling. Also, the larger calculated bandwidths of the bromo-bridged compounds compared to those of the analogous chloro-bridged ones correlate well with the weaker antiferromagnetism found for the latter (Table I).

Why the HOB presents a sizeable bandwidth only for certain values of δ and φ (Figure 2) can be understood from the orbital nature of the weak interactions between the HOMOs of neighboring unit cells. These can be explained by looking at the changes of the overlap integrals between the fragment molecular orbitals of two monomers (Figure 3). For a trigonal bipyramidal structure ($\delta \sim 120°$, circles in Figure 3), the HOMO is the d_{z^2} orbital of the copper atom. At small bridging angles ($\varphi \sim 90°$), where the d_{z^2} orbital of the nearest neighbor sits in the nodal plane of the bridging ligand p orbital, the resulting overlap is zero and, consequently, the HOB shows no dispersion. For larger bridging angles, the interaction between the p orbital of the bridging ligand and the d_{z^2} orbital of the nearest neighbor increases, in keeping with its growing σ character, and the HOB is dispersive. For the square pyramidal case ($\delta \sim 180°$, squares in Figure 3), the HOMO is the $d_{x^2-y^2}$ orbital. At $\varphi \sim 90°$, the interaction between the HOMO of a unit cell and that of its nearest is small but not negligible due to the X–X nonbonded interactions, rapidly dropping to zero as φ increases. Hence, the HOB remains narrow for all values of φ in the square-pyramidal geometry.

In compounds with structures close to a trigonal bipyramid (a, h, and j, Table I), the long Cu–X bond in the equatorial plane is displaced away from the symmetry axis, as shown in **7**. The deviations from the ideal symmetry,

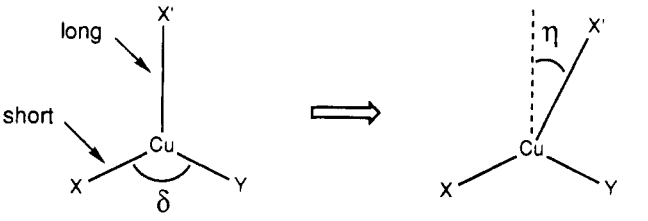

7

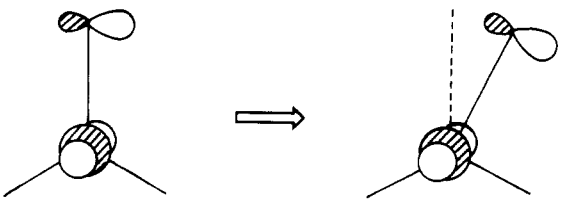

8

defined by the angle η, are 5.5, 10.1, and 3.2° for a, h, and j, respectively. Band calculations on the model compounds show that the bandwidth of the HOB is little sensitive to this distortion, and J_{calc} changes by only -0.1 cm^{-1} for a distortion of 10°. This effect is rather small compared to those of δ and φ studied above. The insensitivity of the bandwidth to asymmetrization can be understood from the shape of the band orbitals for the trigonal bipyramid (Figure 3). If the bridging angle φ is kept constant, the distortion in the equatorial plane does not affect the overlap between the sp hybrid of the bridging ligand and the d_{z^2} orbital of the neighboring Cu atom (**8**) because of its cylindrical symmetry.

Doubly Bridged Chains. The calculated bandwidths for structures **3–5** of $[CuCl_2(\mu\text{-}Cl)_2]^{2-}{}_n$ are plotted in Figure 4, top, as a function of φ. The qualitative behavior is the same in all cases, with only quantitative differences for small angles, suggesting ferromagnetism at some angles ($\varphi \approx 98°$ in our calculations) but antiferromagnetism for both smaller and larger angles. That the shapes of the curves in Figure 4, top, are determined by the overlap between the HOMOs of neighboring units, can be seen in Figure 4, bottom, where the absolute value of the overlap integral between such orbitals is plotted as a function of φ. It is legitimate to ask whether the existence of a minimum in

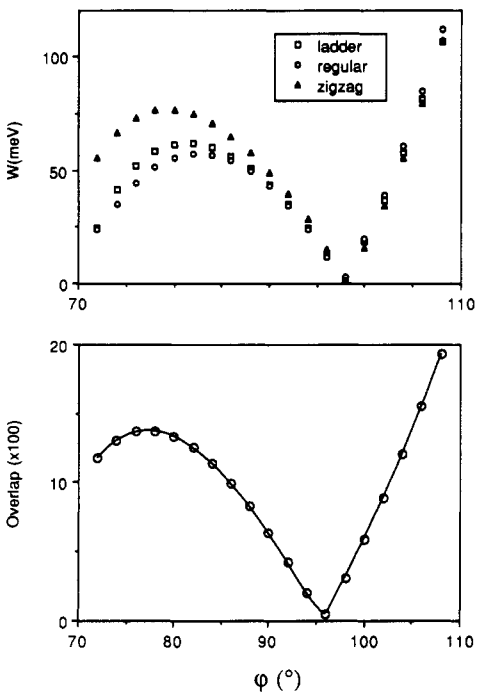

Figure 4. Top: calculated bandwidth of the HOB in $[CuCl_2(\mu\text{-}Cl)_2]^{2-}{}_n$ with structures **3** (ladder), **4** (regular), and **5** (zigzag) as a function of the distortion angle φ (see **6**). The long Cu–Cl distance was taken as 2.8 Å, but similar plots were obtained for other values of this distance. Bottom: overlap integral of the HOMOs of each $CuBr_4^{2-}$ fragment in a dinuclear compound $[CuBr_3(\mu\text{-}Br)]_2^{4-}$ as a function of φ (see Appendix for details).

Figure 4, top, is just an artifact of the computational methodology. A detailed analysis of the overlap integrals between atomic orbitals in neighboring CuY_2X_2 units shows that the only sizeable interaction at $\varphi = 90°$ is that between the σ-donor orbitals of nonbonded X atoms, and it decreases as φ is increased, eventually giving a zero overlap at $\varphi > 90°$. On the contrary, overlap between $d_{x^2-y^2}$ and p_x(Cl) of the neighboring formula unit is switched on for $\varphi > 90°$, as $d_{x^2-y^2}$ moves away from the nodal plane of p_x(Cl). At the end, the position of the minimum bandwidth would depend on several factors: (a) the long Cu–X bond distance, (b) the nature of the ligands, and (c) the size of the atomic orbitals (hence the Slater exponents), but such a minimum is imposed by geometry and should always appear at $\varphi > 90°$.

The overlap between the HOMOs of the neighboring units not only depends on the angle φ but also decreases with increasing Cu–bridge bond distance (r). Therefore, to compare the coupling exchange constants of different compounds, both structural parameters must be taken into account. In such cases it is customary[40,41] to study the trends of J as a function of φ/r. In Figure 5, top, we plot the bandwidth of the HOB as a function of φ/r, calculated for $r = 3.0$ Å. Similar results are obtained for $r = 2.8$ and 3.2 Å but with the minimum displaced, corresponding to $\varphi \approx 98°$ in all cases. A plot of the experimental J values (Figure 5, bottom) appears to be consistent with the calculated bandwidths, although more data would be needed to confirm the form of the calculated curve. The ferromagnetic valley of Figure 5 has been previously observed for dinuclear compounds,[42] but the hill at smaller φ/r has not been noticed before.

(40) Scaringe, R. P.; Hodgson, D. J.; Hatfield, W. E. *Transition Met. Chem.* **1981**, *6*, 340.
(41) Hodgson, D. J. In ref 1, p 497.
(42) Hatfield, W. E. In ref 1, p 555.

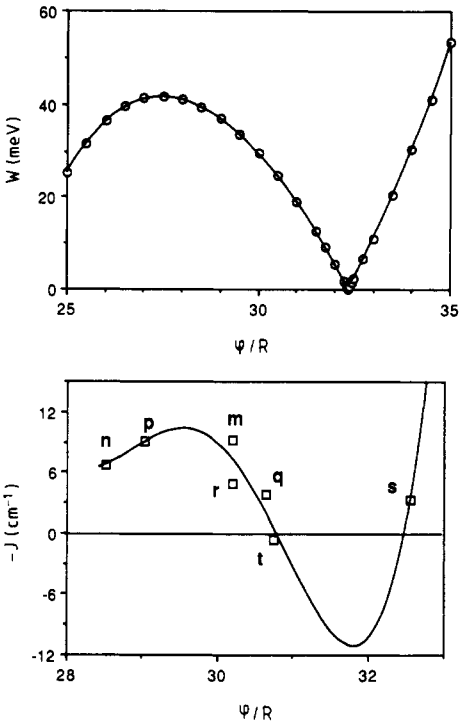

Figure 5. Top: calculated bandwidth of the HOB in $[CuCl_2(\mu\text{-}Cl)_2]^{2-}{}_n$ with structure **4**, as a function of the normalized distortion angle φ/r. Bottom: experimental coupling constants of bis(chloro-bridged) Cu(II) chains with structures **3–5**, as a function of the normalized distortion angle φ/r. The solid line in the lower plot, shown only for illustrative purposes, was obtained through least-squares fitting of the experimental points (see Table II for references).

Table III. Extended Hückel Parameters: Ionization Potentials H_{ii} (eV), Exponents (ζ_i) of the Slater Orbitals, and Coefficients (c_i) for the Double-ζ Expansion of the d Orbitals

atom	orbital	H_{ii}	ζ_i (c_i)
Cu	4s	−11.40	2.20
	4p	−6.06	2.20
	3d	−14.0	5.95 (0.5933), 2.30 (0.5744)
Cl	3s	−26.46	2.03
	3p	−14.96	2.03
Br	4s	−22.07	2.59
	4p	−13.10	2.13

Concluding Remarks. The dependence of the HOB bandwidth on the geometry is in good qualitative agreement with experimental values of the exchange coupling constant J, within a family of analogous compounds with the same bridging atom. However, differences in the values of J equal or smaller than 2 cm^{-1} cannot be accounted for by the approximate model employed.

From Figure 2 one can predict how to improve the antiferromagnetic coupling in this class of compounds by appropriate modification of the geometrical parameters. Hence, we can estimate the upper limit for J_{AF} to be $\sim$−20 and −100 cm^{-1} for X = Cl and Br, respectively, which correspond to a trigonal bipyramid geometry ($\delta \approx 120°$) with a bridging angle $\varphi \approx 180°$.

For doubly bridged chains, ferromagnetism is expected for only a narrow range of bridge angles φ. The available experimental data appear to be consistent with such prediction, although more data would be needed to test our predictions.

Acknowledgment. This work was supported by CICYT through Grant PB86-0272. P.A. is gratefully indebted to the Ministerio de Educación y Ciencia for a grant of the

Plan Nacional de Nuevos Materiales.

Appendix: Computational Details

Electronic band structure calculations[11] within the extended Hückel framework[12] were performed for different geometries on the model compounds listed below. Extended Hückel parameters[18,43] employed in our calculations are collected in Table III.

For singly bridged compounds, the following models were used: $[CuCl_3(\mu\text{-}Cl)]^{2-}_n$ (structure 1, with $120° < \delta < 180°$ and $90° < \varphi < 150°$, at intervals of 10°; structure 2 with $90° < \varphi < 120°$ and $\delta = 360° - 2\varphi$) and $[CuBr_3(\mu\text{-}Br)]^{2-}_n$ (structure 1 with $120° < \delta < 180°$ and $90° < \varphi < 150°$, at intervals of 10°). The following bond distances were used: Cu–X (short) = 2.3 and 2.4 Å, Cu–X (long) = 2.7, 2.8 Å for X = Cl and Br, respectively. For doubly bridged chains, calculations were carried out using $[CuCl_2(\mu\text{-}Cl)_2]^{2-}_n$ as a model (structures **3–5**, with $72° < \varphi < 108°$ at intervals of 2°), with the following bond distances: Cu–Cl (short) = 2.3 Å, and Cu–X (long) = 2.8, 3.0, and 3.2 Å. For the molecular calculations on a dimer $[CuBr_4(\mu\text{-}Br)]_2^{6-}$ (Figure 4, bottom), we used bromide as a bridging ligand instead of chloride, and the long Cu–X bond distance was reduced to 2.6 Å, to exagerate the overlap between the neighboring HOMOs of the dinuclear complex; in that way one can compensate for the neglect of the extended interactions which are taken into account in the band calculations. The bandwidths reported in Table I were calculated for the model compounds $[CuCl_3(\mu\text{-}X)]^{2-}_n$ with the experimental angles and the same bridging atom X as the real compound. Exchange coupling constants were calculated according to eq 2.

(43) Alvarez, S.; Mota, F.; Novoa, J. *J. Am. Chem. Soc.* **1987**, *109*, 6586.

Kinetics and Mechanism of the Crystallization of $Mg_2Al_4Si_5O_{18}$ (Cordierite) from $MgAl_2O_4$ and SiO_2 in the Presence of a Bismuth Oxide Flux

Ryan W. Dupon, Adam C. Tanous, and Mark S. Thompson*

Corporate R&D, Raychem Corporation, 300 Constitution Dr., Menlo Park, California 94025

Received May 11, 1990

Quantitative kinetics and a mechanistic interpretation are presented for the reaction of colloidal SiO_2 and $MgAl_2O_4$ to give $Mg_2Al_4Si_5O_{18}$ in the presence of 2 atom % bismuth oxide. The active flux agent appears to be comprised predominantly of bismuth oxide and silicon oxide. The reaction proceeds through dissolution of the $MgAl_2O_4$ in the siliceous flux to produce an aluminum-substituted quartz stuffed with magnesium ions as an intermediate. The stuffed quartz then converts to cordierite by a first-order process. The rate constant for this conversion is 4.4×10^{-5} s^{-1} at 1000 °C with an activation energy of 70 kcal/mol.

Introduction

The preparation of cordierite ($Mg_2Al_4Si_5O_{18}$) ceramics has attracted considerable attention due in large part to the small thermal expansion coefficient, good strength, and low dielectric constant of $Mg_2Al_4Si_5O_{18}$. Reported preparation methodologies have included the crystallization of glasses with the cordierite composition[1-5] and the hydrolysis of mixed, reactive intermediates such as metal alkoxides[6-8] with the cordierite composition followed by crystallization to the cordierite phase. The conversion mechanism from starting materials to cordierite for each of these processes has been investigated in some detail. Schreyer and Schairer have performed a comprehensive study of the observed phases in the crystallization of glasses in the $MgO–Al_2O_3–SiO_2$ system around the composition of cordierite.[1] Chowdry[7] and Bernier et al.[8] have followed the conversion of hydrolyzed precursors to $Mg_2Al_4Si_5O_{18}$ by X-ray diffraction. As preparative processes both the glass crystallization and sol–gel route have some drawbacks. The glass crystallization process uses common oxide starting materials but requires high temperatures and is inherently a two-step process. The sol–gel process uses expensive, high-energy intermediates, which makes it an expensive and impractical route for bulk oxide materials. We recently reported the preparation of $Mg_2Al_4Si_5O_{18}$ below 1000 °C by the reaction of SiO_2 with $MgAl_2O_4$ in the presence of a small amount of a bismuth oxide flux,[9] while in the absence of bismuth oxide there is no observed reaction. In that paper we described several

* To whom correspondence should be addressed.

(1) Schreyer, W.; Schairer, J. F. Metastable Solid Solutions with Quartz-Type Structures on the Join SiO_2-$MgAl_2O_4$. *Z. Kristallogr.* **1961**, *116*, 60–82.
(2) Gregory, A. G.; Vearey, T. J. The Crystallization of Cordierite Glass. *J. Mater. Sci.* **1971**, *6*, 1312–21.
(3) Zdaniewski, W. "DTA and X-ray Analysis Study of Nucleation and Crystallization of $MgO–Al_2O_3–SiO_2$ Glasses Containing ZrO_2, TiO_2, and CeO_2. *J. Am. Ceram Soc.* **1975**, *58*, 163–69.
(4) Bridge, D. R.; Holland, D.; McMillan, P. W. Development of the Alpha-Cordierite Phase in Glass Ceramics for Use in Electronic Devices. *Glass Technol.* **1985**, *26*, 286–92.
(5) Watanabe, K.; Giess, E. Coalescence and Crystallization in Powdered High-cordierite ($2MgO·2Al_2O_3·5SiO_2$) Glass. *J. Am. Ceram. Soc.* **1985**, *68*, C-102–3.
(6) Moyer, J. R.; Prunier, A. R.; Hughes, N. N.; Winterton, R. C. *Mater. Res. Soc. Symp. Proc.* **1986**, *73*, 117–21.
(7) Gensse, C.; Chowdry, U. Non-Conventional Routes to Glass-Ceramics for Electronic Packaging. *Mater. Res. Soc. Symp. Proc.* **1986**, *73*, 693–703.
(8) Bernier, J. C.; Vilminot, S.; Rehspringer, J. L.; El Hadigui, S.; Poix, P. Sol-Gel Processes and Synthesis of Dielectric Powders for Multilayer Ceramics. *High Tech Ceramics*; Vincenzini, P., Ed.; Elsevier: Amsterdam, 1987; pp 1443–50.
(9) Dupon, R. W.; McConville, R. L.; Musolf, D. J.; Tanous, A. C.; Thompson, M. S. Preparation of Cordierite below 1000 °C via Bismuth Oxide Flux. *J. Am. Ceram. Soc.* **1990**, *73*, 335–339.
(10) JCPDS file no. 12-708.
(11) Perry, R. H., Chilton, C. H., Eds.; *Chemical Engineers Handbook*, 5th ed.; McGraw Hill: New York, 1973; Vol. 3-247.

0897-4756/90/2802-0728$02.50/0